



OPEN

What was the source of the nonseismic tsunami that occurred in Toyama Bay during the 2024 Noto Peninsula earthquake

Hideaki Yanagisawa^{1✉}, Ikuo Abe² & Toshitaka Baba³

In recent years, there have been worldwide reports of massive tsunamis, drawing attention to how tsunamis are intensified by submarine landslides triggered by earthquakes. However, precise data on tsunamis caused by submarine landslides are scarce, leading to insufficient information for a thorough discussion of the characteristics of such tsunamis. On the other hand, during the Noto Peninsula earthquake (M_w 7.5) that occurred in Japan on January 1, 2024, a nonseismic tsunami distinct from those originating from fault ruptures were observed. To investigate its characteristics, we analyzed tide/wave gauge records, video footage, and tsunami trace heights along the coast of Toyama Bay. Furthermore, we validated scenarios capable of reproducing the observed records using an integrated landslide–tsunami model. It was found that assuming the existence of 5 submarine landslides along the underwater canyons of Toyama Bay enabled the precise explanation of multiple types of data. Additionally, our study revealed that submarine landslides occurred approximately 50 s after the earthquake, coinciding with the peak ground shaking in Toyama Bay. Compared to the seismic tsunami originating solely from the Noto Peninsula offshore fault rupture, the subsequent tsunami triggered by submarine landslides amplified the tsunami height by approximately 30% along Toyama Bay.

Keywords Tsunami, Submarine landslide, 2024 Noto Peninsula earthquake, Numerical simulation, Integrated landslide–tsunami model, Tsunami trace height

On January 1, 2024, at 16:10:09 (7:10:09 UTC), a magnitude 7.5 (M_w) earthquake struck the Noto Peninsula, triggering a tsunami¹ (Fig. 1a). According to the Japan Meteorological Agency (JMA), the tsunami, with a wave height of approximately 5 m, was observed in coastal areas near the epicenter of the earthquake, such as Noto town² (Fig. 1b). Additionally, approximately 3 min after the earthquake occurred, a tsunami of 80 cm was observed at a tide gauge station located at the mouth of the Jintsu River in Toyama Bay³, more than 80 km from the epicenter. Initially, we received information from news media that the JMA's preliminary prediction indicated the tsunami would arrive in the Toyama area at 16:20, but the actual arrival time was significantly earlier than this prediction. Some researchers have attempted numerical simulations using earthquake fault models to reproduce the tsunami that arrived within approximately 3 min but have been unable to identify reasonable tsunami waves, suggesting the possibility of a nonseismic tsunami source rather than the earthquake fault⁴.

Following the earthquake, media outlets such as Nippon Hoso Kyokai (NHK) news reported damage that was likely caused by changes in the seafloor topography, such as the loss of crab pots installed at depths of 800 to 1000 m⁵. According to our interview with a fishery cooperative, fixed fishing nets installed in shallow waters at depths of 300 to 400 m were damaged over a wide area of Toyama Bay. Additionally, a seafloor survey conducted by the Japan Coast Guard after the earthquake revealed evidence of a landslide spanning approximately 3.5 km

¹Department of Regional Community Studies, Faculty of Regional Studies, Tohoku Gakuin University, 3-1 Shimizukoji, Wakabayashi-ku, Sendai, Miyagi 984-8588, Japan. ²Department of Social and Environmental Studies, Faculty of Social and Environmental Studies, Tokoha University, 6-1 Yayoicho, Suruga-ku, Shizuoka, Shizuoka 422-8581, Japan. ³Graduate School of Technology, Industrial and Social Sciences, Tokushima University, 2-1 Minami-jyosanjima-cho, Tokushima 770-8506, Japan. ✉email: h-yanagi@mail.tohoku-gakuin.ac.jp

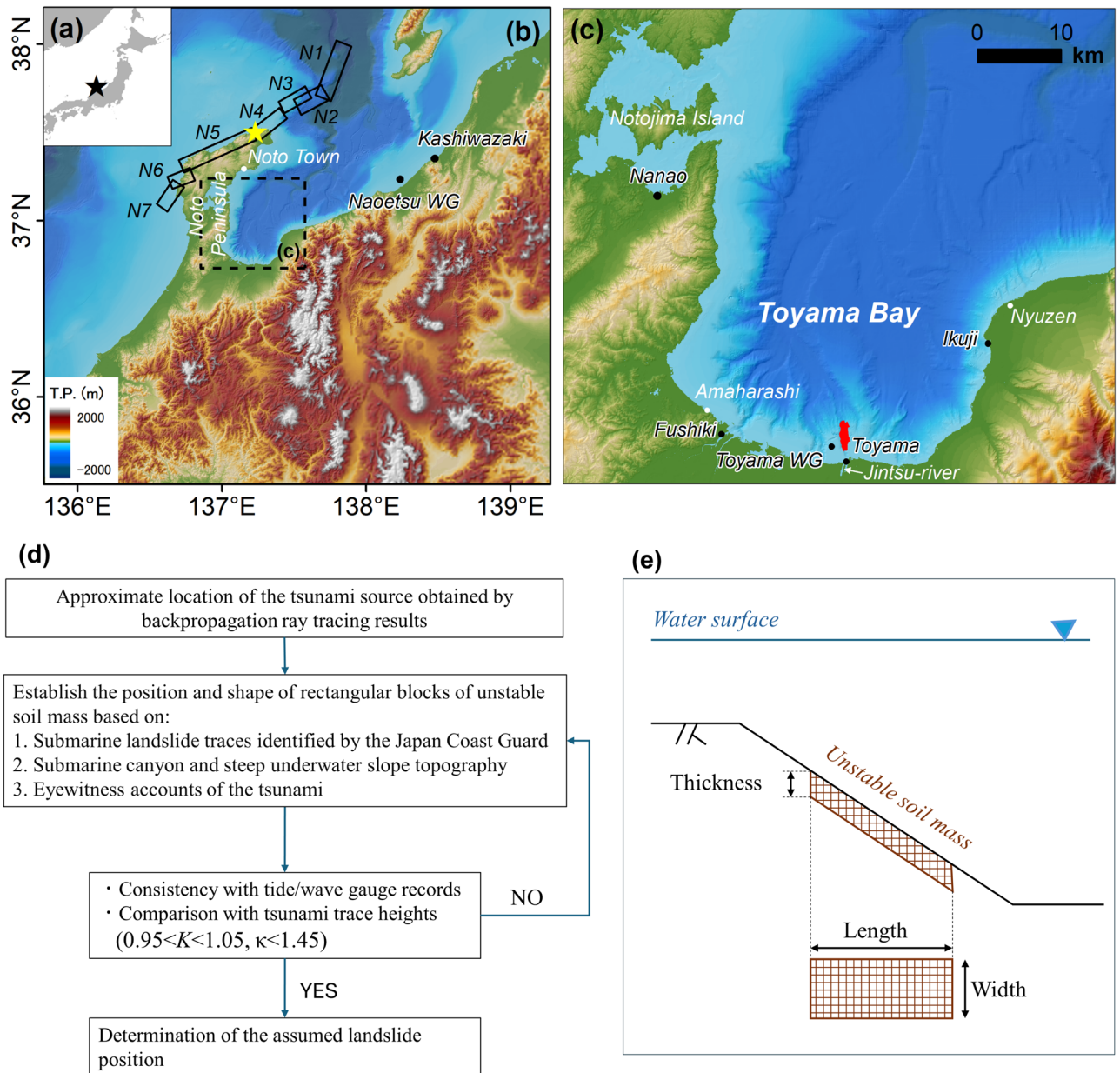


Figure 1. (a) Epicenter of the 2024 Noto Peninsula earthquake. (b) Study area. Rectangles (NT2–NT9) indicating the locations of the faults in the model by Fujii & Stake¹. The star denotes the earthquake epicenter. (c) Map of Toyama Bay. The black dots represent the tide or wave gauge stations. The red shaded area near the Toyama tide gauge station indicates the landslide area detected by the Japan Coast Guard. (d) Flowchart of submarine landslide modeling. (e) Schematic diagram of assumed rectangular blocks of an unstable soil mass.

in the underwater canyon off the Jintsu River⁶ (Fig. 1c). Furthermore, the town of Nyuzen, located northeast of Toyama Bay (Fig. 1c), experienced damage to deep-sea water intake pipes caused by collapses in the offshore canyon⁷. These investigations have suggested that changes in seafloor topography due to events associated with the earthquake, such as submarine landslides or turbidity currents, occurred over a wide area of Toyama Bay.

The underwater topography of Toyama Bay is characterized by a narrow continental shelf that forms steep terrain within a few kilometers from the coast and reaches depths of 1000 m in the deep sea⁸. Many rivers flow into Toyama Bay, including the Oyabe River, Sho River, and Jintsu River on the southwest side and the Joganji River and Kurobe River on the east side, as well as many smaller rivers⁸. Additionally, there are some underwater canyons connected with rivers on the narrow shelf, which converge in the deep sea to form a single large underwater canyon, known as the Toyama deep-sea channel⁸. These underwater canyons are thought to have developed due to events such as erosion by floodwater from land or submarine landslides and turbidity currents associated with earthquakes². In the case of the Noto Peninsula earthquake in 2007 (M_w 6.7), the possibility of landslides on the submarine canyons or slopes of Toyama Bay is also suggested from the analysis of the tsunami arrival time^{9,10}. Based on the seafloor topography of Toyama Bay, there is no active submarine volcano that can

trigger a tsunami¹¹ (Fig. 1b). Although there are some active faults in the bay, there was no evidence of rupturing during either the 2007 or 2024 event^{9,10,12}.

In recent years, some studies have highlighted that submarine landslides can generate devastating tsunamis, causing severe damage to coastal areas^{13–18}. The Aleutian tsunami of 1946^{19,20} and the Papua New Guinea tsunami of 1998^{21,22} are examples of landslide-induced tsunamis that were significantly larger than the tsunami predicted from the earthquake magnitude. Additionally, the tsunami inside Palu Bay, Indonesia, following the 2018 Palu Earthquake was amplified by multiple submarine landslides^{23–25}. However, because submarine landslides occur concurrently with earthquake fault rupture, it is difficult to investigate the characteristics of landslide-induced tsunamis. Moreover, there are no highly accurate observation records of tsunamis generated solely by submarine landslides. Therefore, many aspects of tsunamis caused by submarine landslides remain largely unknown. On the other hand, in the case of the 2024 event, multiple types of data of the nonseismic tsunami remain, including tide/wave gauge records, security camera footage, tsunami witness accounts, and tsunami trace heights. The recorded data on tsunamis generated by submarine landslides could provide valuable insights into the underlying mechanisms controlling such events worldwide. Therefore, in this study, we investigate the characteristics of the nonseismic tsunamis that occurred in Toyama Bay through multiple approaches involving the analysis of recorded datasets, field surveys, and numerical modeling. Using these results, we discuss whether the data observed in this event reflect tsunamis triggered by submarine landslides and the necessity of future disaster prevention measures.

Background for investigating a tsunami source

In this study, to investigate the unknown tsunami source in Toyama Bay, we model the crustal deformation due to the 2024 Noto Peninsula earthquake fault and debris flow caused by submarine landslides as possible sources of tsunami generation. Based on these models, we validate scenarios capable of reproducing the observed records using an integrated landslide–tsunami model^{26,27}.

Modeling of earthquake faults

To investigate the earthquake faults, we utilize the fault model proposed by Fujii & Satake⁴ and calculate the crustal deformation using the method developed by Okada²⁸ (Fig. 1b). In this fault model, the existence of 7 active faults in the northern part of the Noto Peninsula is assumed, and the slip amount of each fault is estimated using joint inversion based on tsunami waveforms observed at tide/wave gauge stations and global navigation satellite system (GNSS) data. However, the wave height of the wave gauge station in Naoetsu was found to be underestimated. The fault directly associated with Naoetsu is considered the N3 fault (Fig. 1b). It was suggested that if the slip amount of N3 is significantly increase, the tsunami at the tide gauge station in Kashiwazaki would be overestimated. Therefore, to balance the tsunami heights between Kashiwazaki and Naoetsu, the slip amount of N3 was reduced. This study focuses on identifying the source of the tsunami that occurred in Toyama Bay. Therefore, we prioritize improving the reproducibility of tsunamis caused by earthquake faults within Toyama Bay. To achieve this, we adjusted the slip amount of N3 (= 6.5 m) to enhance the consistency between the tide/wave gauge records of Toyama Bay and the numerical simulation results. In Toyama Bay, tsunamis caused by submarine landslides arrive earlier than tsunamis caused by earthquake faults, making it possible to evaluate the scale of tsunamis caused by only submarine landslides based on the initial part of the waveforms. Therefore, after determining the scale of tsunamis caused by submarine landslides, it is possible to adjust the slip amount of earthquake faults.

We calculated the tsunamis caused by both the earthquake fault motion and the submarine landslides. Since each represents a different source of the tsunami, it is desirable to simulate the tsunami by considering the timing of each source. According to the Earthquake Catalog of the United States Geological Survey (USGS)¹, the peak moment rate is reached approximately 30 s after an earthquake occurs, and the fault rupture ends approximately 50 s after the earthquake. In this study, we set the rupture onset time for each fault by assuming that the fault rupture propagated uniformly from the epicenter: 30 s for N4 and 5; 40 s for N2 and 3; and 50 s for N1, 6 and 7.

Modeling of submarine landslides

From pre- and postearthquake seafloor topography surveys conducted by the Japan Coast Guard, approximately 3.5 km of submarine landslide traces were identified on both sides of the Jintsu River offshore canyon near the Toyama tide gauge station (Fig. 1c). From the collapse morphology of this landslide, it is inferred that the surface soil layer of steep slopes collapsed due to earthquake shaking and then became liquefied and formed subaqueous debris flows or turbidity currents because sediment deposition due to the landslide is not clearly visible. Although a landslide trace was detected, as mentioned earlier, in this earthquake event, a single submarine landslide or multiple simultaneous submarine landslides may have occurred, potentially contributing to the generation of the tsunami. However, this situation is not fully understood due to the limited understanding of the mechanism of tsunami generation by submarine landslides. Therefore, to explain the multiple observation records collected along Toyama Bay, numerous scenarios must be attempted and tested experimentally. Figure 1d shows the flow adopted to test the submarine landslide scenarios in this study.

First, using the wave-ray tracing method²⁹, we created a backpropagation ray tracing map from the arrival times of tsunamis observed at multiple tide gauge stations around Toyama Bay to roughly identify the source locations of nonseismic tsunamis. The 4th-order Runge–Kutta method was used for the wave-ray tracing solution. The grid size of the bathymetry data used for the analysis was set at 150 m. Next, we determined the position of submarine landslides based on multiple types of data, including the results of the wave-ray tracing method, the landslide traces identified during the Japan Coast Guard survey, the topographic features of the seafloor such as canyons and slopes, and eyewitness accounts gathered from our field survey. In previous studies^{23,24,30}, the slump

type of a landslide has often been assumed to constrain submarine landslide shape. However, the landslides in this event are mainly considered to be surface soil layer collapses around the submarine canyon based on the findings of the Japan Coast Guard. Therefore, in this study, to examine surface soil layer collapse-type landslides, we assumed the placement of an initially rectangular block of unstable soil mass on the seafloor (Fig. 1e). Using this assumption, we simulated the flow of soil mass on the seafloor using a landslide-tsunami integration model^{26,27}. The strike of the rectangular block was set according to the steep slope and the seafloor canyon orientations. This method requires only the width, length, and thickness of the unstable soil mass as shape parameters, enabling the consideration of many scenarios in a straightforward manner. In this study, forward modeling was conducted to develop a model that matches the observed data. The simulation results were compared with observed tide/wave gauge records and tsunami trace heights. If the simulation did not sufficiently match these observations, the submarine landslide scenario was revised. For tide/wave gauge records, we verified whether the computed waveform's water level, wave period, and arrival time trends matched those of the observed waveform. Regarding tsunami trace heights, accuracy was assessed using geometric mean and geometric standard deviation as indicators. This iterative process was repeated hundreds of times until a sufficient match with the observation records was achieved.

Next, we considered the timing of landslide occurrence. In this study, we considered that the submarine landslides were likely to occur when the peak seismic intensity reached Toyama Bay. According to the JMA³¹, it took approximately 20 s for the mainshock of ground shaking to reach Toyama Bay from the epicenter and approximately 30 s to reach the peak moment from the start of the fault rupture¹. Therefore, we added a 50-s time delay for the occurrence of submarine landslides. From video images captured during the tsunami, we can see that the strongest shaking occurred approximately 50 to 60 s after the earthquake, confirming the validity of selecting this time delay.

Results of field surveys

Figure 2 shows the results of tsunami run-up/inundation height measurements at 31 locations along the coast of Toyama Bay. Of these 31 points, 27 were measured for this study, and 4 were measured by the Tokushima University survey team. According to these measurements, on the eastern coast of the bay, the tsunami heights are relatively low, ranging from approximately 1.0 to 1.5 m. On the western coast, however, greater tsunami heights ranging from approximately 1.0 to 2.5 m in height were observed. However, the entire western coast did not uniformly experience larger tsunamis. Localized areas with higher tsunami heights were identified. Particularly

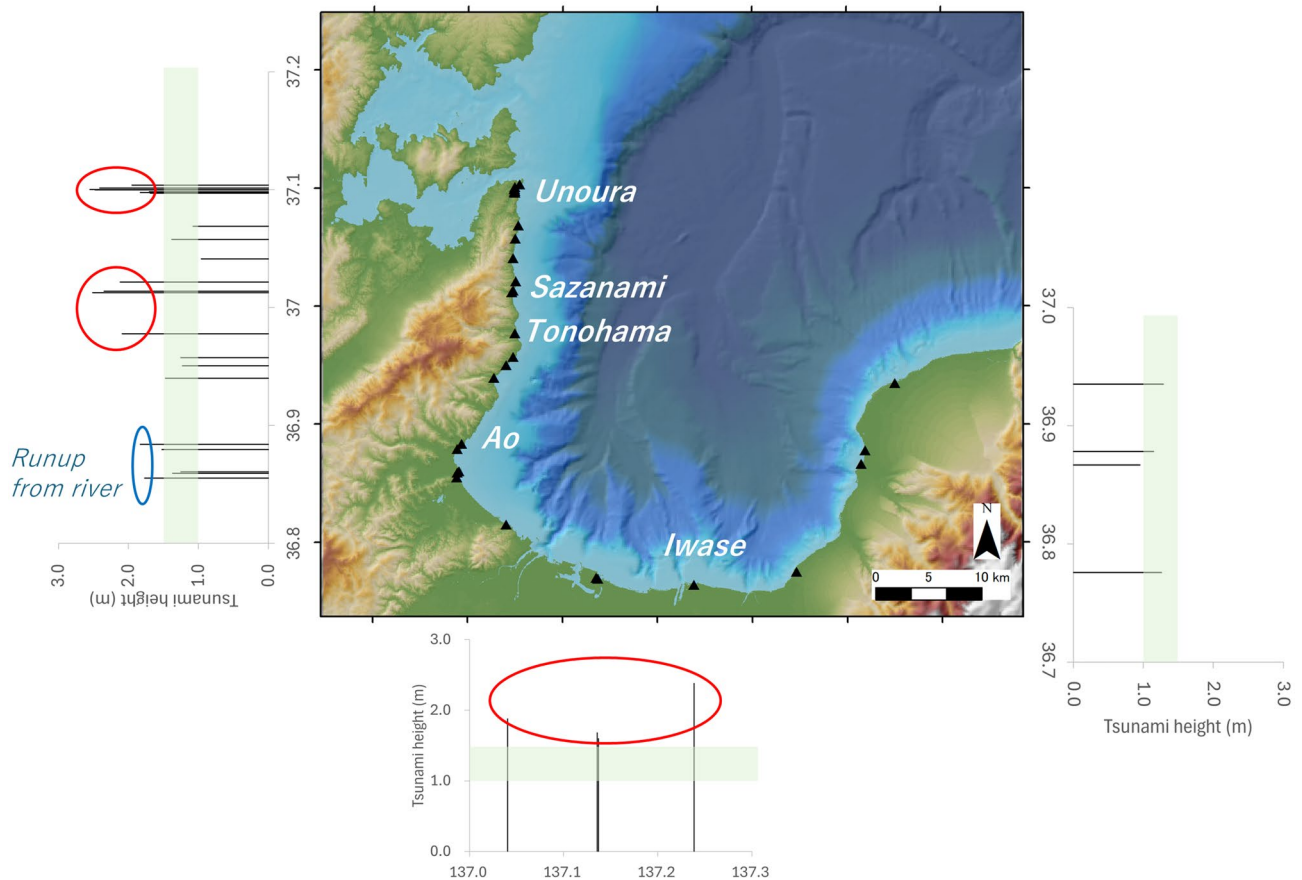


Figure 2. Tsunami height distribution at 31 locations in Toyama Bay. The reference level is Tokyo Peil (T.P.). The green shading in the graph indicates the range of 1.0–1.5 m. Red circles represent locally high tsunami heights. The blue circle indicates the location where the tsunami ran up rivers.

notable areas include Unoura, Sazanami, and Tounohama, where the tsunami heights exceeded 2 m. According to interviews of people present at the Sazanami fishing port, some facilities, such as trucks and forklifts, were partially damaged by the tsunami.

Interviews with local residents revealed that the tsunami curiously reached the Sazanami area within a few minutes after the earthquake occurred, although this area is far from the landslide trace detected by the Japan Coast Guard survey. A resident living in front of the fishing port told us that he began preparing for evacuation in his car immediately after feeling the earthquake shaking and observed the fishing port's boats sinking (not in water) as the water level receded due to the incoming tsunami waves. Typically, eyewitness accounts of tsunami arrival times are vague, and it is difficult to determine specific times. However, in this area, multiple residents remember the unusually early arrival time of the tsunami, which suggests unique circumstances. On the other hand, regarding the Unoura area, there were no eyewitness accounts of tsunamis arriving within a few minutes; instead, a resident told us that there were no receding waves, indicating that the first wave could have been positive. In the Ao area, eyewitness accounts describe the sea receding significantly due to the first tsunami wave, revealing that concrete blocks sunk into the seabed. On the southern side of the bay, higher tsunamis were widely observed, with the maximum height recorded of 2.38 m at Iwase-Hama. From records at the Toyama tide gauge station on the southern side of the bay, receding waves arriving within a few minutes were also observed³. However, the coastline on the southern side of the bay is industrialized, making it difficult to gather eyewitness accounts from residents. Some fishermen present at the ports on the southern side of the bay said that the tsunami did not reach past the coastline, suggesting that there could be not only areas with considerable tsunami heights but also areas with tsunami heights of less than 1.0 to 1.5 m, similar to those on the western side.

Results of the numerical simulations

Figure 3a shows the backpropagation ray tracing results. Considering the time delay of landslide generation, the wavefront lines one minute before tsunami arrival are also indicated. From this map, it can be deduced that nonseismic tsunamis mainly occurred around the southern and western coasts of the bay. In this area, there is no evidence of active faults or volcanic activity during the 2024 event. Therefore, we considered submarine landslides to be nonseismic tsunami sources. Additionally, the final positions of the submarine landslides in each considered scenario determined following the workflow in Fig. 1d are shown in Fig. 3a. At the tide/wave gauge stations of Toyama and Fushiki, the simulated arrival time for the tsunami caused by the submarine landslide is much earlier than 15 to 20 min. Therefore, the impact of the tsunami generated by the seismic fault can be ignored on the waveforms before that time. As a result, adjustments to the landslide scenarios were straightforward.

Figure 3b compares the observed tsunami waveforms at each tide/wave gauge station with the numerical results. Our calculated results are in good agreement with the observed waveforms, confirming that the tsunami was indeed generated by submarine landslides. Furthermore, considering a time delay of 50 s from earthquake onset, the arrival times were also accurately reproduced. In general, a wide area of seafloor movement results in longer-period tsunamis, and lifting the seafloor higher generates higher tsunamis. Therefore, the breadth (width and length) of the landslide source mainly affects the wave period, while the thickness affects the wave amplitude. Furthermore, the location of the tsunami source affects the arrival time. By adjusting each parameter and assuming the position of the unstable soil mass representing the initial landslide condition, we were able to systematically explore solutions from hundreds of scenarios that reproduce the observed tsunami waveforms.

Figure 3c presents the comparison results between the observed tsunami heights and numerical simulations. The results indicate that the calculated tsunami heights within Toyama Bay are underestimated when submarine landslides are not considered (geometric mean $K = 1.28$, geometric standard deviation $\kappa = 1.28$). On the other hand, by incorporating the submarine landslides assumed in this study, the results satisfy the criteria of the Japan Society of Civil Engineers (JSCE)¹⁹ ($K = 1.02$, $\kappa = 1.20$). From the comparison of the K results, it is evident that the tsunami generated by the 2024 Noto Peninsula earthquake was amplified by approximately 30% in Toyama Bay due to the occurrence of submarine landslides.

Results of video analysis

Based on the previous section, we clarified that the tsunami in Toyama Bay was amplified by multiple submarine landslide events. However, there are limited tide gauge records on the western side of Toyama Bay. Therefore, additional information is needed to verify whether our assumptions are accurate for the entire Toyama Bay. For this area, we analyzed footage of the Amaharashi coast (Fig. 1c), where the tsunami arrival was clearly captured (Fig. 4a). According to the analysis results, peaks of the first positive and negative waves were observed 6 min and 10 min after the earthquake occurred, respectively (Fig. 4b). Subsequently, peaks of the positive wave were observed at 12.5 min, followed by the arrival of the maximum wave at 25 min. This maximum wave at 25 min corresponded to the arrival time of the tsunami from the earthquake fault. From these results, it was evident that nonseismic tsunamis also struck the Amaharashi coast, indicating the influence of tsunamis generated by submarine landslides in Toyama Bay.

Effects of each submarine landslide

We next clarify the effects of each assumed submarine landslide (SL1-SL5) on reproducing the observed records. Figure 5 shows the comparison results between the observed tsunami waveforms and calculations by the earthquake fault model with and without submarine landslides (SL1-SL5). Figure 5b presents the results of adding SL1, which is located at the submarine landslide trace found by the Japan Coast Guard. The result with only the earthquake fault model (Fig. 5a) could not reproduce the tsunami waveform up to the second wave at the Toyama tide station, but the trend became reproducible by adding SL1. However, there were disturbances in the waveform, especially at the peak of the first receding wave. Therefore, SL2 was additionally considered to occur

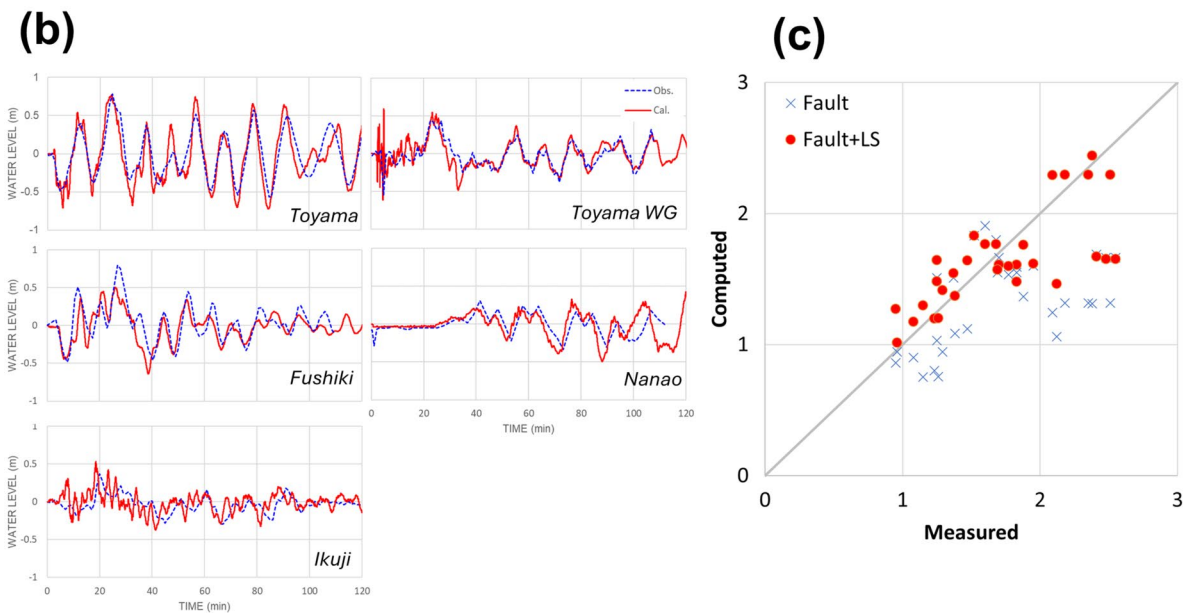
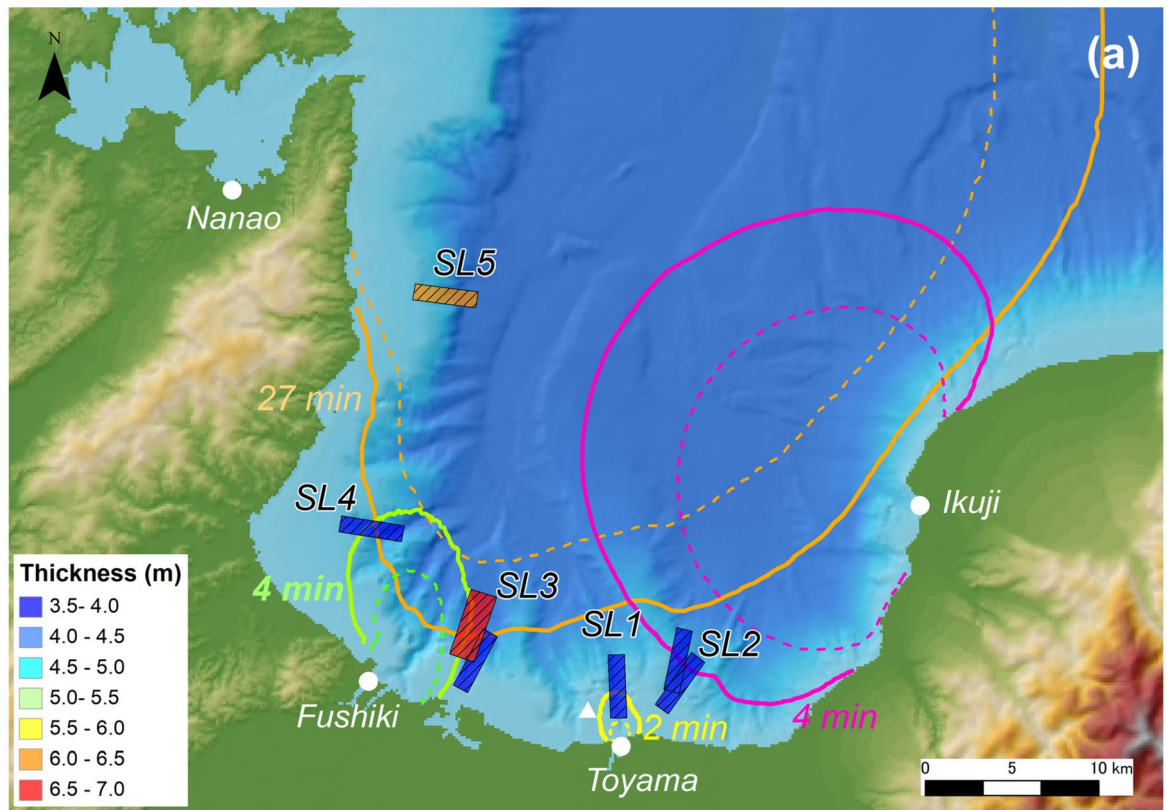


Figure 3. (a) Backpropagation ray tracing map. The solid lines indicate the wave front when the tsunami arrived, while the dotted lines represent the wave fronts one minute before the tsunami arrived. The yellow, green, orange and pink lines indicate the wave fronts determined from the data from the Toyama, Fushiki, Nanao and Ikuji tide gauge stations, respectively. The triangle indicates the Toyama wave gauge station. The rectangles denote the assumed positions of the submarine landslides. Comparison of (b) the observed tsunami waveforms and (c) tsunami trace heights with the computed results.

in the seafloor canyon east of SL1 (Fig. 5c). Although the influence of SL2 was slightly exaggerated due to the balance with the subsequent consideration of SL3, it more clearly reproduced the tendency of the receding wave at the Toyama tide gauge station. On the other hand, with only SL1 and SL2, it was not possible to reproduce the tsunami waveform up to the second to third waves at the Fushiki tide gauge station. This finding implied

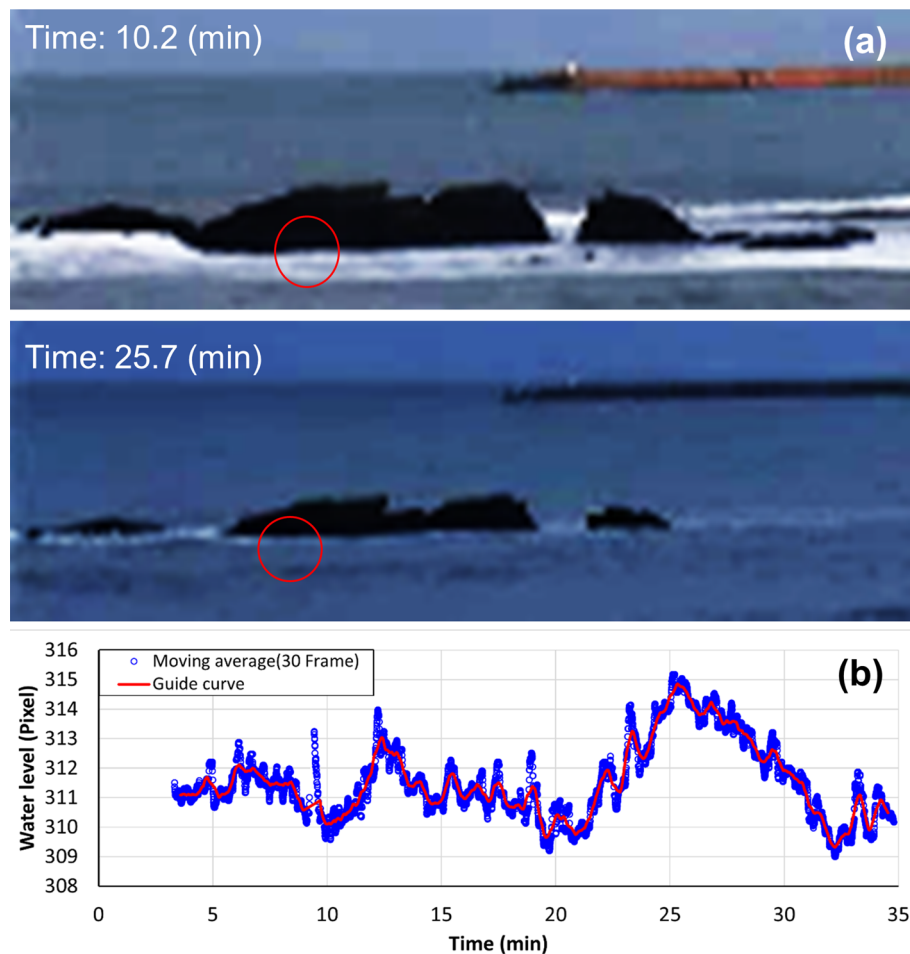


Figure 4. (a) Snapshots of the images after tone adjustment captured at the Amaharashi coast (provided by the Takaoka cable network). The red circle indicates the position of water surface extraction. At this location, it is possible to clearly extract the boundary between the rocks and the water surface. (b) Water surface fluctuations at each frame extracted from the images. The vertical axis indicates the pixel position of the water level from the bottom of the image. The blue dots represent values smoothed with a moving average of 30 frames. The red line represents a guide curve obtained by smoothing the values of the blue dots with a 30-s moving average. The spike at 9 min is due to the influence of aftershock shaking on the video frame.

that other sources were required to reproduce the waveform at Fushiki. Therefore, we assumed that SL3 was an additional submarine landslide at the west canyon of SL1. As a result, the reproducibility of the waveform at the Fushiki tide station was significantly improved (Fig. 5d).

We also considered why the reproducibility of the first wave at the Amaharashi coast was insufficient. In this consideration, the evidence of the strong first receding wave in the Ao area witnessed by a local resident provided some information. To solve this puzzle, we assumed that SL4 was an additional submarine landslide at the seafloor canyon on the west side of Toyama Bay. As a result, the reproducibility of the first positive and negative waves reaching the Amaharashi coast improved, and the situation of the strong first receding wave in the Ao area became consistent (Figs. 5e and 6b). Although the reproduction of tide records greatly improved, the local tsunami heights and arrival times in the Sazanami area revealed during our field surveys did not agree ($K = 1.06$, $\kappa = 1.26$). To address this problem, we considered SL5 to attempt to reproduce the local tsunami heights in the Sazanami area. As a result, while SL5 had little impact on the waveforms at the tide/wave gauge stations (Fig. 5f), it improved the reproducibility of the tsunami heights around the Sazanami area (Fig. 6a).

SL5 was located closer than the front line of the backpropagation ray tracing from the Nanao tide gauge station (Fig. 3a). Tsunamis generated by other landslides propagated faster at depths exceeding 1000 m and then reached the shallow inner bay near the Nanao tide gauge station. These waves caught up with the waves generated by SL5 and then overlapped with them. Therefore, the effects of SL5 on the reproducibility of arrival times at the Nanao tide gauge station were minor. However, changing the position of SL5 had a significant impact on the reproducibility of tsunami waveforms at the Nanao tide gauge station. This was because the reflected waves generated by the first receding wave of SL5 created positive waves, which then overlapped with waves from other landslides or fault models (Fig. 6b). Therefore, the timing of not only the direct waves but also the indirect waves generated by SL5 was critical for the reproducibility of Nanao's waveform. Additionally, there were eyewitness

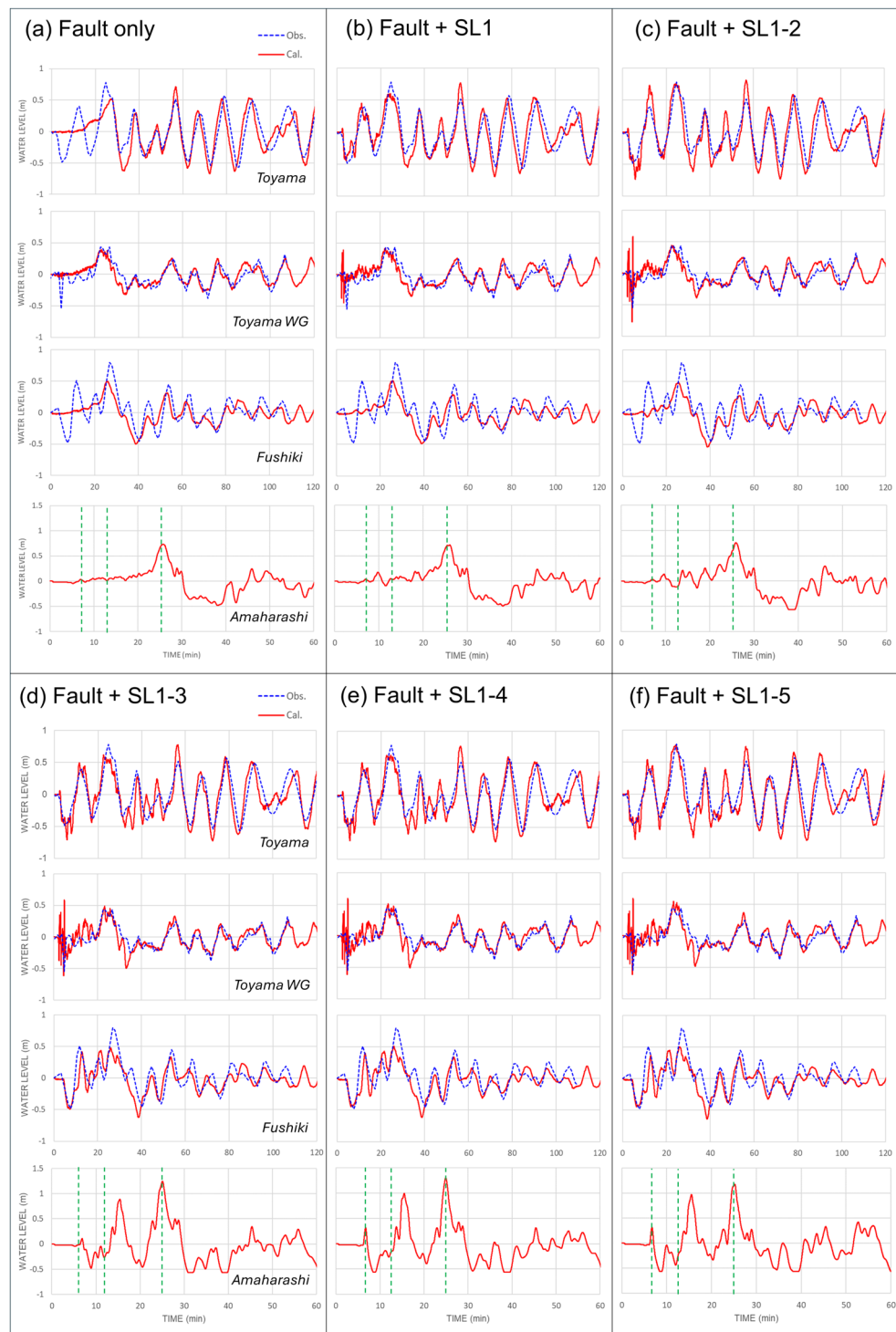


Figure 5. Comparison of simulation results and observed data for each assumed landslide scenario: (a) fault only, (b) fault and SL1, (c) fault and SL1-2, (d) fault and SL1-3, (e) fault and SL1-4, and (f) fault and SL1-5. The green lines depicted on the graph for Amaharashi indicate the peak times of the positive waves obtained through image analysis (Fig. 4b).

accounts of the initial arrival of positive waves in Unoura, which made it difficult to assume a submarine landslide near the offshore area of Unoura because landslides generate receding waves landward (Fig. 6b). This information provided strict constraints for determining the position of SL5. However, adding SL5 could underestimate tsunami heights in the Unoura area, requiring further adjustments in the future (Fig. 6a).

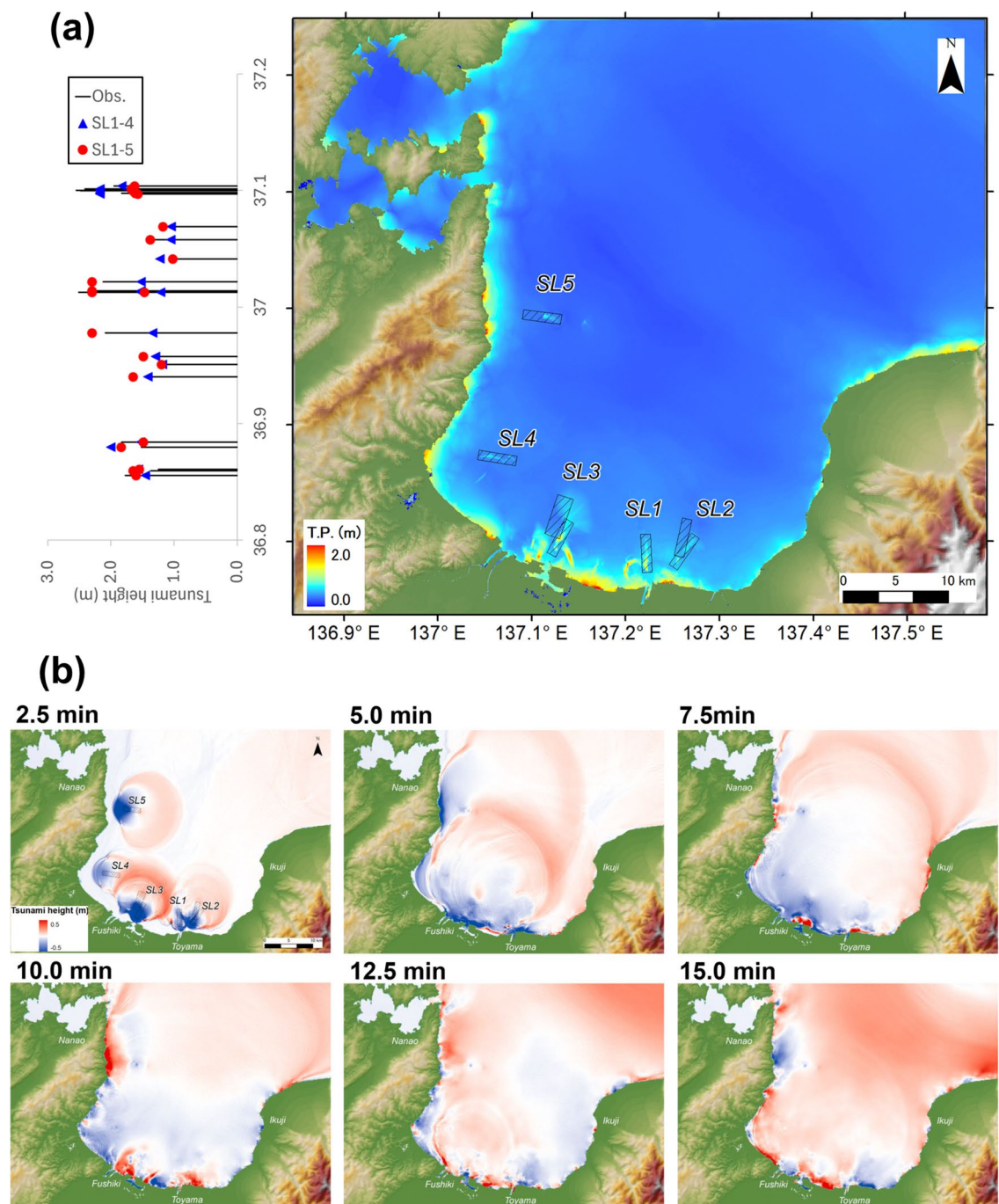


Figure 6. (a) Comparison of simulation results with and without SL5. The right panel shows the maximum tsunami height for the fault with landslides SL1-5. (b) Snapshots of tsunami water level distribution.

We further estimated the root mean square error (RMSE) between observed tide/wave gauge data and computed results, both with and without submarine landslides, during the 30 min following the earthquake. The RMSE values are 0.16, 0.22, and 0.16 for Toyama, Fushiki, and Toyama WG, respectively, while the values without considering submarine landslides are 0.28, 0.25, and 0.15, respectively. Near the source of the landslide, the landslide's behavior is unstable, resulting in no improvement in the RMSE value at the Toyama wave gauge. However, significant improvements were noted in the RMSE values for Toyama and Fushiki.

Discussion

Here, we discuss the impact of the time delay between the submarine landslides and earthquake fault rupture. The cases with and without a time delay between the earthquake rupture and submarine landslides are compared in Fig. 7. From the comparison of Fig. 7a and b, it was observed that adding a 50-s time delay to the occurrence of submarine landslides could align the waveform phase at the Toyama tide gauge station for up to 15–20 min. The

Toyama tide gauge station was mainly affected by SL1, which was constrained by the position of the submarine landslide trace detected by the Japan Coast Guard. Thus, reproducing the observed records without considering the time delay was not possible. From these results, we validated the 50-s delay of submarine landslides after earthquake occurrence. Furthermore, Fig. 7c shows the results when considering the time delay of the earthquake fault rupture. Introducing a time delay of the earthquake fault rupture slightly improves the reproducibility of the tsunami waveforms from the earthquake faults.

Finally, we conducted simulations to reproduce the observed data collected in this study, considering not only the earthquake fault model but also submarine landslide scenarios with SL1 to SL5. Figure 8 shows the simulation results regarding the movement of the soil mass from the submarine landslides after 3 h. According to interviews with fishermen, crab traps were washed out on both the west and east sides of the deeper sea area with depths greater than 800–1000 m in the bay. While the specific locations of the crab traps were not disclosed to the public due to business secrecy, it was noted that the approximate initial locations of the crab traps could be consistent with the simulated direction of the soil mass movement from the submarine landslides. Although our model cannot replicate the transition phenomena of soil masses such as those from landslides to mudflows involving abundant water, actual soil masses from landslides may transform into turbidity currents as they move, gradually descending to more distant areas.

In the eastern part of Toyama Bay, a deep-sea water intake pipe in Nyuzen was damaged by submarine landslides. However, according to the information from the investigation by Nyuzen town, the scale of the submarine landslides might be relatively small compared to that of SL1–SL5. In the Nyuzen area, we also confirmed no evidence of significantly amplified tsunami heights from earthquake faults (Fig. 2). Thus, we infer that the effects of the submarine landslide off Nyuzen were minor in Toyama Bay, although further research is necessary to understand the actual situation and assess the risk of future events.

This study revealed that multiple submarine landslides amplified the tsunami in Toyama Bay triggered by the 2024 Noto Peninsula earthquake. The seafloor topography of Toyama Bay results in a high potential for submarine landslides to amplify tsunamis following large earthquakes. Currently, submarine landslide risk is not considered in Japan's tsunami hazard maps or evacuation plans. Therefore, it is essential to investigate and consider the future risks associated with submarine landslides.

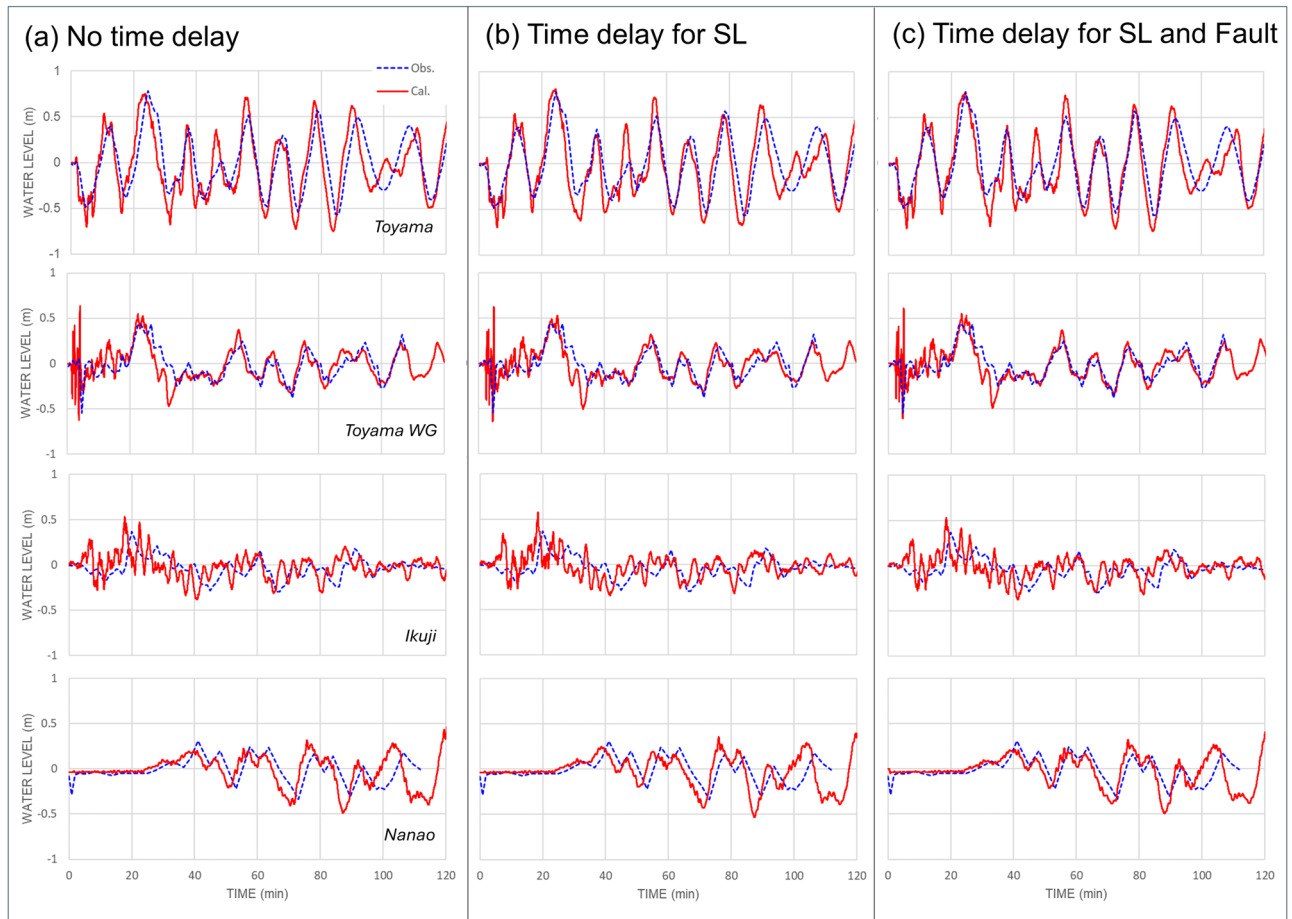


Figure 7. Influence of time delay with landslide and fault occurrence: (a) no time delay, (b) time delay for the submarine landslides, and (c) time delay for submarine landslides and fault.

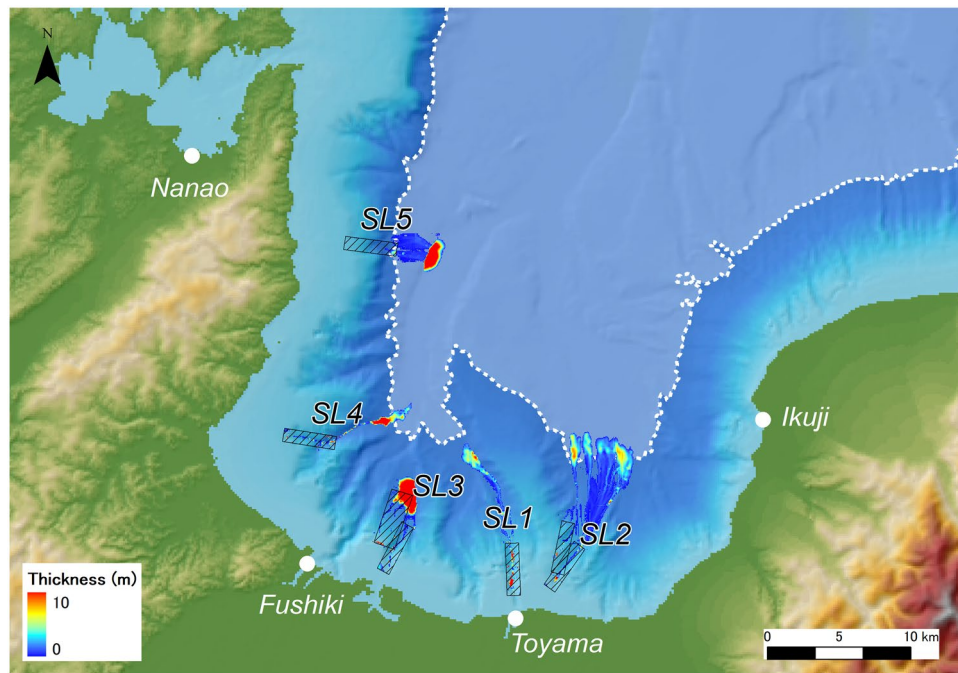


Figure 8. The simulation results regarding the movement positions of the soil mass from the submarine landslides after 3 hours. The white shaded area indicates the sea area deeper than 800 m where the crab pots were lost.

Concluding remarks

In this study, we examined a nonseismic tsunami that occurred in Toyama Bay following the 2024 Noto Peninsula earthquake through field surveys, numerical analysis and video analysis. Consequently, by hypothesizing 5 landslides near submarine canyons within Toyama Bay and conducting numerical simulations, we were able to explain multiple observational datasets. A comparison between numerical simulations with and without submarine landslides revealed that approximately 30% of the tsunami height was amplified by the occurrence of submarine landslides during this event. Furthermore, it was inferred that the submarine landslides did not collapse immediately after the fault rupture but rather began collapsing approximately 50 s after the earthquake occurred.

The method proposed in this study, utilizing a rectangular block of unstable soil mass, was found to be both simple and capable of adequately recreating observed records with sufficient accuracy. Considering the risks of submarine landslides in vulnerable regions, this method enables extensive calculations of tsunami scenarios incorporating submarine landslides and thus is valuable for designing tsunami disaster prevention measures.

Methods

Field surveying

We conducted field surveys targeting the coastal areas of Toyama Bay on three occasions: January 20–23, February 18–20, and February 28–March 1, 2024. The surveys included measurements of tsunami trace heights and interviews regarding eyewitness accounts of the tsunami. To determine tsunami heights, we relied on watermarks, coastal debris arrival positions, video recordings, and eyewitness accounts to ascertain the inundation or run-up heights of the tsunami. In regions where ocean swells were significant, such as in the northeastern part of the bay, the height of the tsunami may have been influenced by ocean waves other than the tsunami itself. Therefore, we selected measurement locations that were minimally affected by waves, such as fishing ports and those behind breakwaters, as much as possible. Moreover, we considered coastal debris only when its movement was captured in videos or when there were eyewitness accounts of debris movement, as it could include debris transported by typhoons or high waves before the tsunami. We conducted ground-level measurements using Trimble R2 GNSS or Pentax G6 GNSS devices. The GNSS data obtained from our surveys were analyzed based on data from the website of the GNSS Earth Observation NETWORK System (GEONET) of the Geospatial Information Authority of Japan (GSI) to determine elevations³². All data were referenced to Tokyo Peil (T.P.) which is elevation above the average sea level in Tokyo Bay. All method were approved by the Human Subjects Research Ethics Committee of Tohoku Gakuin University. Our surveys were carried out in accordance with relevant guidelines and regulations of Tohoku Gakuin University. During these surveys, interviews were conducted after explaining that it was university research aimed at investigating the tsunami and obtaining informed consent from all subjects. Additionally, no personally identifiable information was collected in these surveys.

Numerical model

To analyze the behavior of submarine landslides and tsunamis in Toyama Bay, numerical simulations were conducted using a two-layer model based on shallow-water wave theory. In this model, the upper layer represents the water mass (tsunami), and the lower layer represents the soil mass (landslide). This allows for numerical simulations that consider the interaction between submarine landslides and tsunamis^{25,26,33,34}.

Upper layer:

$$\begin{aligned} \frac{\partial}{\partial t}(\eta_1 - \eta_2) + \frac{\partial M_1}{\partial x} + \frac{\partial N_1}{\partial y} &= 0, \\ \frac{\partial M_1}{\partial t} + \frac{\partial}{\partial x}\left(\frac{M_1^2}{D_1}\right) + \frac{\partial}{\partial y}\left(\frac{M_1 N_1}{D_1}\right) + gD_1 \frac{\partial \eta_1}{\partial x} + \frac{\tau_{x1}}{\rho_1} + INTF_x &= 0, \\ \frac{\partial N_1}{\partial t} + \frac{\partial}{\partial x}\left(\frac{M_1 N_1}{D_1}\right) + \frac{\partial}{\partial y}\left(\frac{N_1^2}{D_1}\right) + gD_1 \frac{\partial \eta_1}{\partial y} + \frac{\tau_{y1}}{\rho_1} + INTF_y &= 0. \end{aligned} \quad (1)$$

Lower layer:

$$\begin{aligned} \frac{\partial \eta_2}{\partial t} + \frac{\partial M_2}{\partial x} + \frac{\partial N_2}{\partial y} &= 0, \\ \frac{\partial M_2}{\partial t} + \beta \frac{\partial}{\partial x}\left(\frac{M_2^2}{D_2}\right) + \beta \frac{\partial}{\partial y}\left(\frac{M_2 N_2}{D_2}\right) + gD_2\left(\alpha \frac{\partial D_1}{\partial x} + K_0 \frac{\partial D_2}{\partial x} - \frac{\partial h_2}{\partial x}\right) + \frac{\tau_{x2}}{\rho_2} - \alpha INTF_x &= 0, \\ \frac{\partial N_2}{\partial t} + \beta \frac{\partial}{\partial x}\left(\frac{M_2 N_2}{D_2}\right) + \beta \frac{\partial}{\partial y}\left(\frac{N_2^2}{D_2}\right) + gD_2\left(\alpha \frac{\partial D_1}{\partial y} + K_0 \frac{\partial D_2}{\partial y} - \frac{\partial h_2}{\partial y}\right) + \frac{\tau_{y2}}{\rho_2} - \alpha INTF_y &= 0, \end{aligned} \quad (2)$$

where η is the surface elevation, M and N are the discharge in the x and y directions, t is the time, h is the water depth, D is the flow depth ($= \eta + h$), g is the gravitational acceleration, α is the ratio of the densities of the water and soil masses (ρ_1/ρ_2), τ is the shear stress, $K_0 = \alpha + (1 - \alpha)K_s$, K_s is the lateral soil pressure ratio, β is the correction factor of momentum (1.25 in the debris flow), and $INTF$ indicates the interface resistance. Subscripts 1 and 2 represent the upper and lower layers, respectively. We used the following equations to estimate the interface resistance:

$$INTF_x = f_{inter} \bar{u} \sqrt{\bar{u}^2 + \bar{v}^2}, \quad (3)$$

$$INTF_y = f_{inter} \bar{v} \sqrt{\bar{u}^2 + \bar{v}^2},$$

where \bar{u} and \bar{v} are the relative velocities in the x and y directions, respectively, and f_{inter} is the coefficient of interface resistance. For the bottom shear stress of the upper layer, we used the Manning formula as well as a general tsunami simulation³⁵. A Manning coefficient of 0.025 was employed to reproduce the behavior of the tsunami³⁵. Yanagisawa et al.²⁵ simulated the behavior of landslides using the model employed in LS-RAPID³⁶ as the friction law for the soil mass, successfully reproducing the extent of sediment deposition and tsunami heights associated with the 1792 Mount Mayuyama sector collapse. On the other hand, Ioki et al.²⁶ proposed a practical model for the friction law of the soil mass based on the Coulomb viscosity model³⁷, combining the Coulomb law and the Manning formula. This model successfully simulated the sediment deposition and tsunami behavior resulting from the 1741 Oshima-Oshima sector collapse. Below are the equations for the x and y directions of the model proposed by Ioki et al.²⁶:

$$\frac{\tau_{x2}}{\rho_2} = \frac{gn_2^2}{D_2^{7/3}} M_2 \sqrt{M_2^2 + N_2^2} + \frac{M_2 g D_2 \tan \Phi}{\sqrt{M_2^2 + N_2^2}}, \quad (4)$$

$$\frac{\tau_{y2}}{\rho_2} = \frac{gn_2^2}{D_2^{7/3}} N_2 \sqrt{M_2^2 + N_2^2} + \frac{N_2 g D_2 \tan \Phi}{\sqrt{M_2^2 + N_2^2}},$$

where Φ is the internal friction angle and n_2 is the Manning coefficient of the lower layer. In the equations, on the right side, the first term significantly influences the current velocity of the soil mass, while the second term determines the cessation of soil mass movement.

Previous studies, such as those of Sassa et al.³⁸ and Iverson & Denlinger³⁹, have proposed equations primarily designed to simulate landslides on land. However, the landslide examined by Ioki et al.²⁶ in the 1741 Oshima-Oshima sector collapse occurred predominantly underwater. Therefore, the model must be used to regulate the current velocity and cessation of debris flows under saturated conditions beneath seawater. Considering the focus of this study on submarine landslide behavior, the model proposed by Ioki et al.²⁶ was selected. Regarding the Manning coefficient of the soil mass movement, Kawamata³⁴ utilized $n_2 = 0.12$ to reproduce tsunami waveforms in laboratory experiments. Additionally, Ioki et al.²⁶ conducted a parameter study targeting the Oshima-Oshima sector collapse and evaluated $n_2 = 0.15$ as the optimal value. Since these values are nearly the same, we used $n_2 =$

0.15 for our simulation. Compared to the collapse in Oshima–Oshima, the submarine landslides in Toyama Bay, which are assumed to be surface soil layer collapses, may have greater fluidity. This could make it more difficult to stop soil mass movement. However, it is difficult to determine parameters related to the cessation of soil mass movement because the depositional area of the soil mass during this event is still not clear. Therefore, in this study, we assumed a smaller value for Φ (1.0°) than that set by Ioki et al.²⁶ as the estimated value. The density of the soil mass was set to $\rho_2 = 2.0 \text{ g/cm}^3$ based on Sassa et al.³⁸. The lateral soil pressure ratio K_s was assumed to be 1.0, assuming full saturation under water. However, few previous studies have examined the parameters of the friction law based on the Coulomb viscosity model for tsunamis caused by submarine landslides, resulting in uncertainties in the accuracy of the parameters. Although these parameters may not significantly represent the observed wave period and waveform shape, they could affect the tsunami wave height caused by submarine landslides. In other words, the balance between the thickness of the unstable soil mass and the friction parameter determines the tsunami height. Therefore, the thickness of the unstable soil mass may not necessarily match the actual landslide thickness, and it is necessary to clarify the relationships among the actual landslide shape, friction parameters, and thickness of the unstable soil mass in the future.

The region including the open ocean shown in Fig. 1b is defined as Region 1, while the region shown in Fig. 1c is defined as Region 2. Numerical simulations were conducted by constructing 2 nesting grids for each region⁴⁰. The grid sizes for each region were set to 150 m and 50 m, and the time steps were set to 0.3 s and 0.1 s, respectively. The simulation time was set to 3 h from the occurrence of the earthquake. To evaluate the reproducibility of tsunami heights via numerical simulations, the geometric mean K and geometric standard deviation κ were utilized as indicators²⁷.

$$\log K = \frac{1}{n_0} \sum_{i=1}^{n_0} \log K_i, \quad (5)$$

$$\log \kappa = \left[\frac{1}{n_0} \sum_{i=1}^{n_0} (\log K_i)^2 - (\log K)^2 \right]^{1/2},$$

where n_0 represents the number of points, i denotes the point number, and $K_i = x_i/y_i$, where x and y are the measured tsunami height and computed tsunami trace height, respectively. According to the criteria of the JSCE⁴¹, the accuracy criteria are defined as $0.95 < K < 1.05$ and $\kappa < 1.45$.

Video analysis

In the video analysis, we first extracted images from the video frame by frame and adjusted the tone. Next, we used the Canny method to extract the edges of the water surface using the Open Computer Vision Library (OpenCV). Then, we selected points in the image where water level fluctuations could be clearly observed and graphed the fluctuations by tracking the pixel height of the images (Fig. 4a,b). We used the values of the data averaged over 30 images (approximately 10 s) for the graph.

Data availability

For tide gauge records at Toyama station, digital data are available from the UNESCO/Intergovernmental Oceanographic Commission (IOC) website (<https://www.ioc-sealevelmonitoring.org/>). Tide gauge records at Nanao were digitized from figures on the JMA website, while tide gauge records for Fushiki and wave gauge records off the coast of Toyama were digitized from figures on the MLIT's Port and Harbor Bureau from the NOWPHAS website (<https://www.mlit.go.jp/kowan/nowphas/>). Tide gauge data at Ikuji and video footage near the Kurobe area were provided by the Ministry of Land, Infrastructure, Transport and Tourism, Kurobe Office of the River. Video footage at the Shinminato Arena, Iwase-Hama and Amaharashi coasts was obtained from the NHK Toyama broadcast station, Cable Television Toyama Inc. and Takaoka Cable Network Co., Ltd., respectively. The OpenCV library is available from their website (<https://opencv.org/>).

Received: 12 May 2024; Accepted: 31 July 2024

Published online: 06 August 2024

References

1. USGS Earthquake Hazards Program, M 7.5 - 2024 Noto Peninsula, Japan Earthquake. <https://earthquake.usgs.gov/earthquakes/eventpage/us6000m0xl/finite-fault>. Accessed 05 Aug 2024.
2. JMA Press Releases. Results of on-site tsunami surveys conducted by the Japan Meteorological Agency's Rapid Response Team (JMA-MOT) for the 2024 Noto Peninsula Earthquake. https://www.jma.go.jp/jma/press/2401/26a/20240126_tsunamichousakekka.pdf (2024). Accessed 05 Aug 2024.
3. JMA Press Releases. the 2024 Noto Peninsula Earthquake - Third Report. <https://www.jma.go.jp/jma/press/2401/01c/kaisetsu202401012130.pdf> (2024). Accessed 05 Aug 2024.
4. Fujii, Y. & Satake, K. Slip distribution of the 2024 Noto Peninsula earthquake (MJMA 7.6) estimated from tsunami waveforms and GNSS data. *Earth Planets Space* **76**, 44 (2024).
5. NHK NEWS. Earthquake Causes Significant Impact on Winter Delicacy Red Snow Crab Fishing at Toyama's Shinminato Fishing Port. <https://www3.nhk.or.jp/news/html/20240110/k10014316791000.html> (2024). Accessed 05 Aug 2024.
6. Japan Coast Guard Press Releases. Confirmation of Submarine Landslide Traces in Toyama Bay (Second Report). https://www.kaiho.mlit.go.jp/info/kouhou/r6/k240311_2/k240311_2.pdf (2024). Accessed 05 Aug 2024.
7. NHK NEWS. Toyama Bay: Earthquake Causes Severing of Intake Pipes for Deep-sea Water from the Ocean Depths. <https://www3.nhk.or.jp/news/html/20240213/k10014356871000.html> (Accessed 05 Aug 2024).
8. Nakajima, T., Mikio Satoh, M. & Yukinobu Okamura, Y. Channel-levee complexes, terminal deep-sea fan and sediment wave fields associated with the Toyama deep-sea channel system in the Japan Sea. *Mar. Geol.* **147**, 25–41 (1998).

9. Abe, I., Goto, K., Imamura, F. & Shimizu, K. Numerical simulation of the tsunami generated by the 2007 Noto Hanto Earthquake and implications for unusual tidal surges observed in Toyama Bay. *Earth Planets Space* **60**, 133–138 (2008).
10. Namegaya, Y. & Satake, K. Tsunami generated by the 2007 Noto Hanto earthquake. *Earth Planets Space* **60**, 127–132 (2008).
11. Hydrographic and Oceanographic Department, Japan Coast Guard. Submarine Volcano Database. <https://www1.kaiho.mlit.go.jp/kaiikiDB/list-2.htm> (Accessed 05 Aug 2024).
12. Hiramatsu, Y., Moriya, K., Kamiya, T., Kato, M. & Nishimura, T. Fault model of the 2007 Noto Hanto earthquake estimated from coseismic deformation obtained by the distribution of littoral organisms and GPS: Implication for neotectonics in the northwestern Noto Peninsula. *Earth Planets Space* **60**, 903–913 (2008).
13. Baba, T., Matsumoto, H., Kashiwase, K., Hyakudome, T., Kaneda, Y. & Sano, M. Micro-bathymetric evidence for the effect of submarine mass movement on tsunami generation during the 2009 Suruga Bay earthquake. *Japan Submarine Mass Movements and Their Consequences Edited by Y. Yamada et al, Advances in Natural and Technological Hazards Research*, **31**, 485–495 (2012).
14. Tappin, D. R. *et al.* Did a submarine landslide contribute to the 2011 Tohoku tsunami?. *Mar. Geol.* **357**, 344–361 (2014).
15. Okamura, Y., Nishizawa, A., Fujii, Y. & Yanagisawa, H. Accretionary prism collapse: A new hypothesis on the source of the 1771 giant tsunami in the Ryukyu Arc, SW Japan. *Sci. Rep.* **8**, 13620 (2018).
16. Ren, Z., Liu, H., Li, L., Wang, Y. & Sun, Q. On the effects of rheological behavior on landslide motion and tsunami hazard for the Baiyun Slide in the South China Sea. *Landslides* **20**(8), 1599–1616 (2023).
17. Ren, Z., Higuera, P. & Li-Fan Liu, P. On tsunami waves induced by atmospheric pressure shock waves after the 2022 Hunga Tonga-Hunga Haʻapai volcano eruption. *J. Geophys. Res. Oceans* **128**(4), e2022JC019166 (2023).
18. Løvholt, F., Pedersen, G., Harbitz, C. B., Glimsdal, S. & Kim, J. On the characteristics of landslide tsunamis. *Philos. Trans. R. Soc. A Math. Phys. Eng. Sci.* **373**(2053), 20140376 (2015).
19. Okal, E. A., Plafker, G., Synolakis, C. E. & Borrero, J. C. Near-field survey of the 1946 Aleutian tsunami on Unimak and Sanak Islands. *Bull. Seismol. Soc. Am.* **93**, 1226–1234 (2003).
20. von Huene, R., Kirby, S., Miller, J. & Dartnell, P. The destructive 1946 Unimak near-field tsunami: New evidence for a submarine slide source from reprocessed marine geophysical data. *Geophys. Res. Lett.* **41**, 6811–6818 (2014).
21. Okal, E. A., Borrero, J. C. & Synolakis, C. E. Solving the puzzle of the 1998 Papua New Guinea tsunami: The case for a slump. *Solut. Coast. Disasters* **2002**, 863–877 (2002).
22. Synolakis, C. *et al.* The slump origin of the 1998 Papua New Guinea Tsunami. *R. Soc. Lond. Proc. Ser. A* **458**, 763–789 (2002).
23. Nakata, K., Katsumata, A. & Muhari, A. Submarine landslide source models consistent with multiple tsunami records of the 2018 Palu tsunami, Sulawesi, Indonesia. *Earth Planets Space* **72**, 44 (2020).
24. Nagai, K. *et al.* Consideration of submarine landslide induced by 2018 Sulawesi earthquake and tsunami within Palu Bay. *Coast. Eng. J.* **63**, 446–466 (2021).
25. Sepúlveda, I., Haase, J. S., Carvajal, M., Xu, X. & Liu, P. L. Modeling the sources of the 2018 Palu, Indonesia, tsunami using videos from social media. *J. Geophys. Res. Solid Earth* **125**(3), e2019JB018675 (2020).
26. Yanagisawa, H. Numerical simulation of the 1792 Mt. Mayuyama collapse and the resulting tsunami using two-layer model. In *AOGS 15th Annual Meeting* (2018).
27. Ioki, K., Tanioka, Y., Yanagisawa, H. & Kawakami, G. Numerical simulation of the landslide and tsunami due to the 1741 Oshima-Oshima eruption in Hokkaido, Japan. *J. Geophys. Res. SE* **124**, 1991–2002 (2019).
28. Okada, Y. Surface displacement due to shear and tensile faults in a halfspace. *Bull. Seismol. Soc. Am.* **75**, 1135–1154 (1985).
29. Satake, K. Effects of bathymetry on tsunami propagation: Application of ray tracing to tsunamis. *Pure Appl. Geophys.* **126**, 27 (1988).
30. Lo, P. H. Y. & Liu, P. L. F. A simplified approach for efficiently simulating submarine slump generated tsunamis. *Coast. Eng.* **184**, 104343 (2023).
31. JMA Press Releases. The time from emergency earthquake alert provision to the arrival of the main shock (2024).
32. Geospatial Information Authority of Japan (GSI). the GNSS Earth Observation NETWORK System (GEONET). https://www.gsi.go.jp/ENGLISH/geonet_english.html (Accessed 05 Aug 2024).
33. Imamura, F., Hashi, K. & Imteaz, M. A. Modeling for tsunamis generated by landsliding and debris flow. In *Tsunami Research at the End of a Critical Decade* (ed. Hebenstreit, G. T.) 209–228 (Springer, 2001).
34. Kawamata, K. *et al.* Model of tsunami generation by collapse of volcanic eruption: The 1741 Oshima-Oshima tsunami. In *Tsunamis* (ed. Satake, K.) 79–96 (Springer, 2005).
35. Japan Society of Civil Engineers (The Tsunami Evaluation Subcommittee, The Nuclear Civil Engineering Committee). Tsunami assessment method for nuclear power plants in Japan. Japan Society of Civil Engineers (2002). https://committees.jsce.or.jp/ceofnp/system/files/JSCE_Tsunami_060519.pdf (Accessed 05 Aug 2024).
36. Ajmera, B. *et al.* LS-RAPID manual with video tutorials. In *Progress in Landslide Research and Technology, Volume 1 Issue 1, 2022. Progress in Landslide Research and Technology* (eds Sassa, K. *et al.*) 209–228 (Springer, 2023).
37. Johnson, A. M. *Physical Processes in Geology* Vol. 577 (Freeman Cooper, 1970).
38. Sassa, K., Nagai, O., Solidum, R., Yamazaki, Y. & Ohta, H. An integrated model simulating the initiation and motion of earthquake and rain induced rapid landslides and its application to the 2006 Leyte landslide. *Landslides* **7**, 219–236 (2010).
39. Iverson, R. M. & Denlinger, R. P. Flow of variably fluidized granular masses across three-dimensional terrain 1. Coulomb mixture theory. *J. Geophys. Res.* **106**, 537–552 (2001).
40. Goto, C., Ogawa, Y., Shuto, N. & Imamura, F. *IUGG/IOC Time Project, numerical method of tsunami simulation with the Leap-Frog scheme. IOC Manuals and Guides, UNESCO, Paris* (1997).
41. Aida, I. Reliability of a tsunami source model derived from fault parameters. *J. Phys. Earth* **26**, 57–73 (1978).

Acknowledgements

The video data used in this study were provided by Wataru Ikeda of the NHK Toyama Broadcasting, Yumi Suzuki of the Cable TV Toyama, and Tetsuya Kishi of the Takaoka Cable Network. Tide gauge records in Ikuji and video data around the Kurobe area were provided by Yuichi Takamura of the Ministry of Land, Infrastructure, Transport and Tourism, Kurobe Office of River. Kunio Nishimoto of the Shinminato Fisheries Cooperative provided information on port and fishery damage. Kiyoshi Wakabayashi and Yuki Hiroshima of Nyuzen town provided information for the underwater surveys performed near the Nyuzen area. Additionally, we conducted interviews with residents and individuals associated with fishing ports regarding the tsunami. We sincerely thank everyone who kindly cooperated with us despite being busy with postdisaster recovery activities. This research was supported by JSPS KAKENHI (grant numbers 23H00528 and 22KK0010).

Author contributions

H.Y. and I.A. proposed the topic and designed the research. H.Y. and T.B. conducted the field surveys. I.A. conducted the image analysis. H.Y. conducted the numerical modeling. All authors participated in discussions and approved the final manuscript.

Competing interests

The authors declare no competing interests.

Additional information

Correspondence and requests for materials should be addressed to H.Y.

Reprints and permissions information is available at www.nature.com/reprints.

Publisher's note Springer Nature remains neutral with regard to jurisdictional claims in published maps and institutional affiliations.

Open Access This article is licensed under a Creative Commons Attribution-NonCommercial-NoDerivatives 4.0 International License, which permits any non-commercial use, sharing, distribution and reproduction in any medium or format, as long as you give appropriate credit to the original author(s) and the source, provide a link to the Creative Commons licence, and indicate if you modified the licensed material. You do not have permission under this licence to share adapted material derived from this article or parts of it. The images or other third party material in this article are included in the article's Creative Commons licence, unless indicated otherwise in a credit line to the material. If material is not included in the article's Creative Commons licence and your intended use is not permitted by statutory regulation or exceeds the permitted use, you will need to obtain permission directly from the copyright holder. To view a copy of this licence, visit <http://creativecommons.org/licenses/by-nc-nd/4.0/>.

© The Author(s) 2024